Numerical Investigations of an Integrated Phase-Change-Material Solar Collector

Z. Bouhssine[1], M. Faraji[1], M. Najam[1] and M. El Alami[1,2]

Abstract: The objective of this study is to optimize the thermal performance of a solar collector. The solar collector is coupled to a building slab with a PCM layer. A mathematical model for the thermal behavior of the studied system is developed using the enthalpy method. The model parameters are defined and the resulting equations are solved iteratively. Several simulations were carried out to optimize the proposed heating system. The results show that the inlet temperature fluctuations are less pronounced than those at the outlet.

Keywords: Solar collector, heat balance, optimization, PCM, heating, concrete, building.

Nomenclature

S total radiation received by the collector, [W/m^2]
D outside diameter of the tubes, [m]
L distance between the glass and the absorber, [m]
E absorber thickness, [m]
q_u useful flux transferred to the fluid, [W/m^2]
T_{fi} fluid inlet temperature, [K],[˚C]
T_{fo} fluid outlet temperature, [K],[˚C]
T_f melting temperature, [K],[˚C]
T_a ambient temperature, [K],[˚C]
T_c internal temperature under the slab, [K],[˚C]
T_{in} building internal temperature, [K],[˚C]
k thermal conductivity, [W/m K]
h_{in} internal convective coefficient under the slab, [W/m^2 K]
f liquid fraction

[1] Laboratory of Physical Materials, Microelectronics, Automatics and Heat Transfer, Faculty of Science, Hassan II University, Casablanca-Morocco.
[2] Corresponding Author. E-mail: m.elalami@etude.univcasa.ma; m.elalami@fsac.ac.ma

w	distance between the tubes, [m]
A_c	area of solar collector, [m^2]
U_L	overall conductance, [W/m^2 K]
c_p	heat capacity, [J/kg K]
R_b	transposition factor
F_R	conductance factor of absorber
H_b	light, [W/m^2]
H_d	diffuse radiation, [W/m^2]
H	global radiation, [W/m^2]

Greek symbols

β	tilt angle by degrees
$\dot{m}$	water flow rate, [kg/s]
ω	hour angle by degrees
δ	declination
φ	latitude
ΔH	latent heat of melting, [KJ/kg]
ρ	density, [kg/m^3]
φ_{sa}	radiation absorbed by the absorbent, [W/m^2]

Subscripts

m	PCM
b	concrete
s	solid
l	liquid

1   Introduction

The daily performance of a solar collector depends on thermo-physical parameters of the heating fluid (the fluid inlet and outlet temperatures, storage temperature), the components of the system (overall coefficient of the solar collector's heat losses) and the meteorology conditions (solar radiation, temperature, humidity etc.). Detailed analysis of a solar collector is a complex task, due to the high number of parameters affecting its performances. In the last 40 years, several dynamic procedures have been developed and tested using numerical approaches, to get the solar collector behavior without making the whole complex and expensive experimental

testing generally adopted in the approaches to the steady state. In this context, a great effort has been made in recent years by [Tagliafico et al. (2014)], also, by [Hakem et al. (2008)] to improve the potential of prediction of dynamic models of solar collectors. In the same sense, [Gao et al. (2013)] made a comparison of thermal performances between two types of solar collectors. [Wei et al. (2013)] propose an improvement of the structure of a solar plan where a transient heat transfer model was developed to calculate the performance of the solar collector, the temperatures of the water, of the glass and of absorber. [Handoyo et al. (2013)], also, [Tadili and Bargach (2005)] showed that the choice of orientation and the tilt angle of the solar collector also contribute to the increase of these thermal performances. [Probst and Roecker (2007)] conducted an investigation on the integration of solar thermal systems in the building in order to improve their qualities and potential to the eventual new users. Within the same framework, [Yang et al. (2013)] study the integration of the solar plan ceramic. The results show that when the solar collector is placed on the sloping roofs during the construction, the thermal efficiency of the solar system in ceramic is more than 50%. Also, the use of solar collectors integrated in the building in solar air conditioning systems should be limited to situations where the availability of the roof is insufficient when applied in sub - tropical regions such as Hong Kong deduced by [Fong et al. (2012)]. [Kosny et al. (2007)] have studied the importance of the PCM and uses thereof to stabilize the temperature inside the building. Thus, the best places for the integration of the PCM is on the surfaces of interior walls, ceilings, or floors. The passive construction solutions with PCMs reduce the energy consumption for heating and cooling, and for increasing inside thermal comfort due to the reduced inlet temperature fluctuations by [Soares et al. (2013)]. [Mohamed Rady and Eric Arquis (2010)] studied the phase changing behavior of granular composites by using differential scanning calorimetry (DSC) and a modified T-history method. [Prud'homme and El Ganaoui (2007)] gave a review about some numerical and experimental problems related to the solid/liquid phase change.

In the present work, a parametric study is developed in two parties to optimize the thermal performance of the plan solar collector built into a concrete slab in the presence of a PCM in January in Casablanca. In the first part, several simulations were conducted to improve the geometric parameters of the solar collector (diameter of the tubes, the absorber thickness, etc.), the inclination of the solar collector, and the flow rate of the fluid in the system. Also in the second part, important simulations were made to optimize the thermo-physical properties of the PCM. The results show that the optimization of the characteristic parameters of the solar collector allows an increase of its efficiency of 17%. In addition, the optimization of thermo-physical parameters of the PCM ensures the conditions for thermal comfort

for the building.

2   Physical model

Fig.1.a. provides an overview of the proposed model, it is subwoofer fixed, iso-lated from the sides, carrying forward a glass surface. The inside of the subwoofer includes an absorbent plate copper tinted in a dark coating that maximizes the ab-sorption of solar radiation. The return of the energy captured is done by passage of a heat transfer fluid (water) in contact with the metal surface. A layer of the PCM is directly connected to the subwoofer, which is fixed to the slab. A representative area defines the location of the layer of the PCM in the system and the various parameters on the thermal behavior of the solar collector, Fig.1.b.
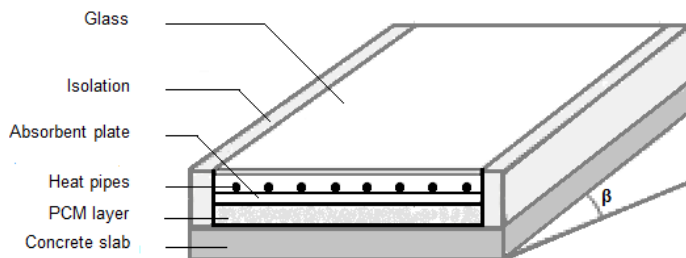
Figure 1.a: The physical model.
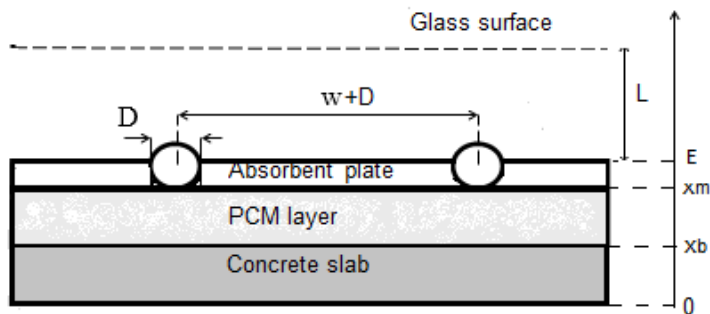
Figure 1.b: The physical model.

2.1   Assumptions

For the mathematical formulation of the problem, the following assumptions were adopted:

- Hourly steady state;

- One-dimensional heat transfer;

- For radiation GLO, the sky is a black body at T_{sky};

- Thermal conductivity of concrete is assumed to be constant;

- The PCM is homogeneous and isotropic. Natural convection in the PCM is neglected;

- Interfacial resistors between the different layers of the system are neglected.

2.2   Equations

Global radiation received by the solar collector [12]:

$$S = \left(\frac{1 + \cos(\beta)}{2} \right) H_d + 0.2 \left(\frac{1 - \cos(\beta)}{2} \right) H + R_b H_b \tag{1}$$

With:

$$R_b = \frac{\sin(\delta)\sin(\phi - \beta) + \cos(\delta)\cos(\phi - \beta)\cos(\omega)}{\sin(\delta)\sin(\phi) + \cos(\delta)\cos(\phi)\cos(\omega)} \tag{2}$$

Heat balance of the solar collector:

$$A_c \phi_{sa} = Q_u + Q_p + Q_s \tag{3}$$

In steady state:

$$Q_u = A_c \left[\phi_{sa} - U_L(T_p - T_a) \right] \tag{4}$$

The global coefficient of heat losses to the atmosphere U_L is the sum of the forward heat losses U_t, the heat losses to the rear U_b and laterally heat losses U_e. It is given by [13]:

$$U_L = U_t + U_b + U_e \tag{5}$$

The useful flux transferred to the fluid is:

$$q_u = F_R \left[\phi_{sa} - U_L \left(T_{fi} - T_a \right) \right] \tag{6}$$

Furthermore, the conductance factor F_R defined in equation (7) represents the ratio between the power actually retrieved and power that we would have obtained if the temperature of the fluid was equal to the inlet temperature of the fluid, [14].

$$F_R = \frac{\dot{m}c_p}{AU_L} \left[1 - \exp\left(\frac{-AU_L F'}{\dot{m}c_p} \right) \right] \tag{7}$$

F′ represents the thermal resistance between the absorber and the ambient by the thermal resistance between the fluid and the ambient.

The average temperature of the fluid is given by:

$$\bar{T}_f = T_{fi} + \frac{\frac{q_u}{A}}{U_L F_R} \left(\frac{1 - F_R}{F'} \right) \tag{8}$$

The outlet temperature of the fluid is expressed by:

$$T_{fo} = \left(T_{fi} - T_a - \frac{\phi_{sa}}{U_L} \right) \exp \left(\frac{-A U_L . F'}{\dot{m} c_p} \right) + \frac{\phi_{sa}}{U_L} + T_a \tag{9}$$

The energy equation under transient conditions in the slab in concrete/PCM is written using the enthalpy method [15]:

$$\rho c_p \frac{\partial T}{\partial t} = \frac{\partial}{\partial x} \left(k \frac{\partial T}{\partial x} \right) - \rho \Delta H \lambda \frac{\partial f}{\partial t} \tag{10}$$

The second term takes account of the latent heat associated with phase change when it occurs while f represents the liquid fraction given by:

$$\begin{cases} f = 1 & T > T_f \\ f = 0 \quad \text{if} \quad T < T_f \\ 0 < f < 1 & T = T_f \end{cases} \quad \text{With} \quad \begin{cases} \lambda = 0 & \text{In concrete} \\ \lambda = 1 & \text{In PCM} \end{cases} \tag{11}$$

The boundary conditions are as follows:

$$x = x_m, \quad -k_m \left. \frac{\partial T}{\partial x} \right|_x = q_u \tag{12}$$

$$x = 0, \quad -k_b \left. \frac{\partial T}{\partial x} \right|_x = h_{in} (T_c - T_x) \tag{13}$$

Equality of the flow and temperature at the interface:

$$k_+ \left. \frac{\partial T}{\partial x} \right|_x = k_- \left. \frac{\partial T}{\partial x} \right|_x, \quad T_+ = T_- \tag{14}$$

The thermo-physical properties of the PCM are as follows:

$$k_m = f . k_{m,l} + (1 - f) k_{m,s}, \quad (\rho c_p)_m = f . (\rho c_p)_{m,l} + (1 - f) (\rho c_p)_{m,s} \tag{15}$$

Interfaces 'i' between two different materials ('+' /'-'), the properties are estimated by the method of harmonic averages [15]:

$$k_i = \frac{k_+ k_- (\delta_+ + \delta_-)}{k_+ \delta_- + k_- \delta_+} \tag{16}$$

With δ_+ is the separation between the interface and the first node of the material '+' and δ - is the separation between the interface and the last node of the material '-'.

Initial conditions

The system is subject to the climatic conditions of Casablanca-Morocco, during the month of January, Fig.2.
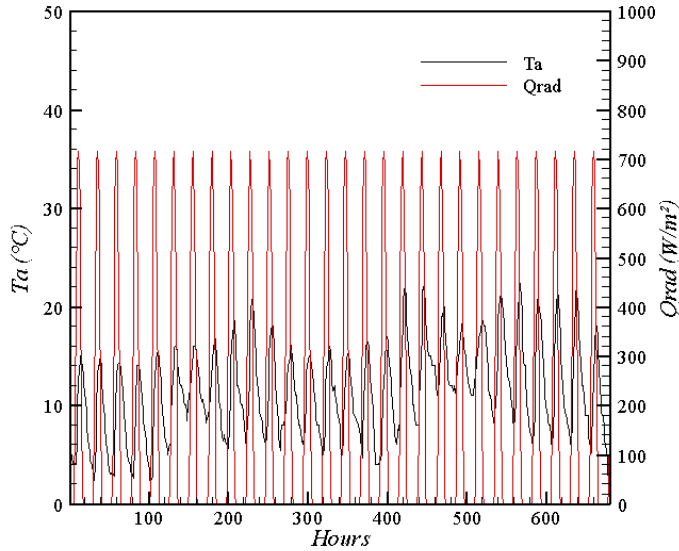

Figure 2: Climatic conditions of Casablanca-Morocco in January.

An iterative calculation on the absorber and the glass, temperatures used to calculate the coefficient of overall heat losses U_L.

The system of equations obtained is numerically integrated on a set of control volumes, Patankar [15].

Table 1: Geometric Configuration of the solar collector.

β	D (m)	w (m)	E (m)	L (m)	$\dot{m}$ (kg/s)
0°	0.0218	0.08316	0.0035	0.04	0.005

Fig.3. illustrates the influence of the time on the precision of the calculations step. Note that the time step influence on the liquid fraction. The most suitable time for the stability of the results is 1 s.

Table 2: Thermo-physical properties of the PCM.

k_m (W/m K)	c_{pm} (J/kg K)	ρ_m (kg/m^3)	ΔH (KJ/kg)	T_f(°C)
1.9	1000	1800	200	22

Table 3: Thermo-physical properties of the concrete slab.

k_b (W/m K)	c_{pb} (J/kg K)	ρ_b (kg/m^3)
1.5	838	2200

Table 4: Time step optimization.

Δt_0(s)	Δt_1(s)	Δt_2(s)	Δt_3(s)	Δt_4(s)	Δt_5(s)
20	20	5	2	1	0.5
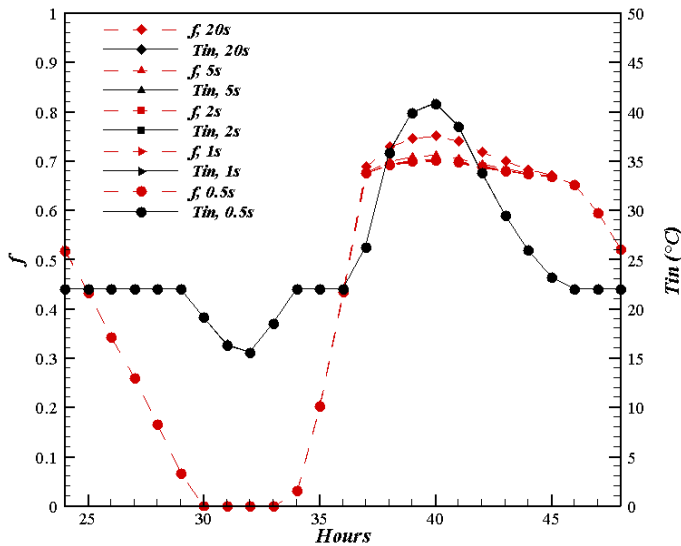
Figure 3: Time step effect on the problem solution.

3   Results and discussion

In this study, we proceed to the optimization of the solar collector with PCM. Tilt angle β, the diameter of the tubes D, the distance between the tubes w, the thickness of the absorber E, the distance between the glass and the absorber L, the water

flow rate and the PCM thermo-physical parameters are the control parameters implemented.

3.1   Solar collector optimization

To optimize the solar collector, we did the following steps: At Solar noon, we examined the effect of geometric parameters of the sensor by varying one parameter and fixing the other, on the maximum useful heat flux and the outlet temperature of the fluid.

Tilt angle β

The variation of the tilt angle β has an appreciable effect on the thermal behavior of the solar collector. Indeed, by increasing β from 0˚ to 75˚, the maximum useful heat flux transferred to the coolant fluid, rebounds from 351.76 W/m^2 to 588.73 W/m^2 and decreases to 567.08 W/m^2, Fig.4.a. In this range of β, the outlet temperature of the heating fluid increases from 56.7˚C to 80.2˚C and decreases to 78.09˚C at solar noon. Up of $\beta = 60$˚, each of heat flux and outlet temperature decrease and their related curves show a maximum for $\beta = 60$˚, a value which we recommend in winters to optimize the radiation received by the surface of the solar collector.
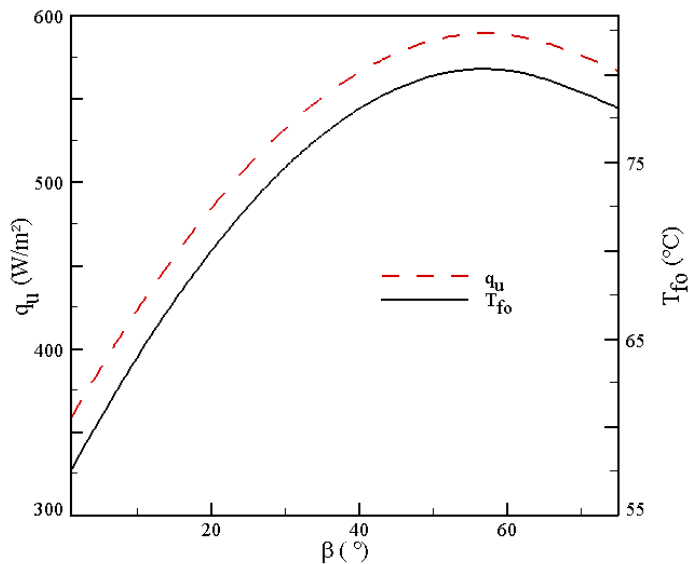
Figure 4.a: Variation of the useful flux and the outlet temperature as functions of the tilt angle at solar noon.
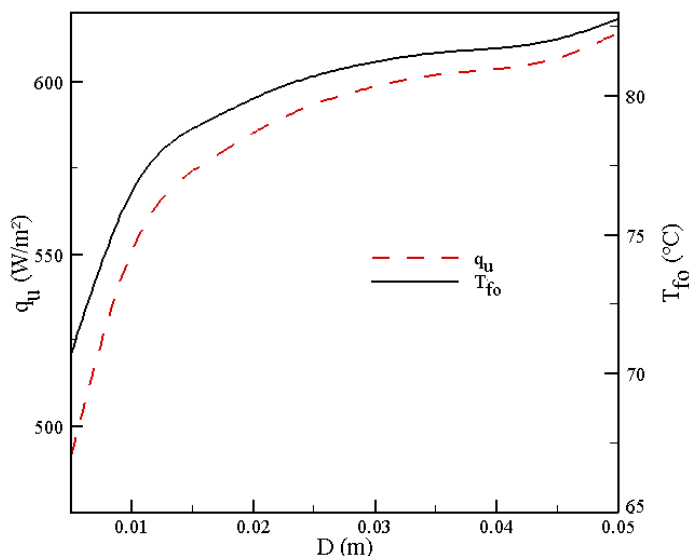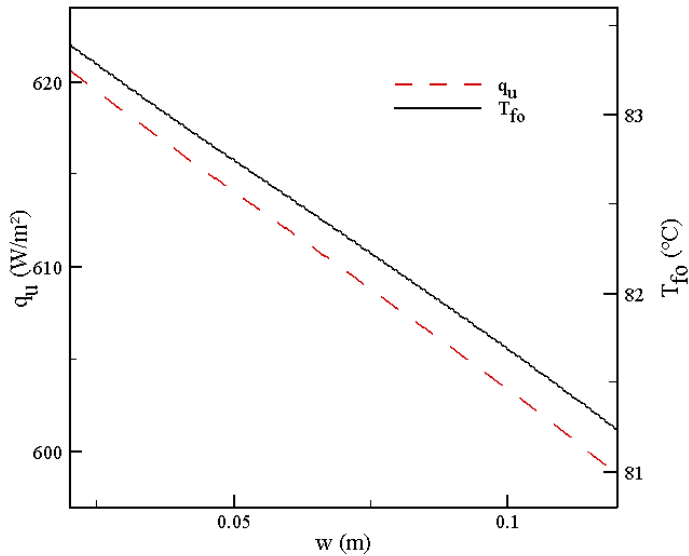
Figure 4.b: Variation of the useful flux and the outlet temperature as a function of the diameter of the tubes at solar noon.

Diameter of the tubes D

In this section, we fixed the angle inclination as $\beta=60°$ and we varied the tube diameter D in the range of 0.005m $\leq$ D $\leq$ 0.05m. Generally, the increase of the tube diameter influences the thermal behavior of the solar collector. Indeed, when D increases, the flow area increases which leads to the reduction of the fluid velocity, resulting in a dwell time of more slowly in the tubes. So, by varying D from 0.005 m to 0.05 m, the maximum useful heat flux transferred to the coolant flowing, rebounds from 492.11 W/m^2 to 607.04 W/m^2, Fig.4.b. The increase in the diameter D of the tubes contributes, also, to the increase of the outlet temperature of the coolant, from 70.6°C to 82.05°C at solar noon.

We will take D=0.04 m as diameter of the tubes, available on the catalogs.

Distance between the collector tubes w

The increase of w from 0.02 m to 0.12 m creates a reduction in the maximum useful flux assigned to the heat transfer fluid, which decreases, from 620.60 W/m^2 to 598.81 W/m^2 as shown in Fig.5.a. The increase of the distance between the tubes also contributes to a slight decline of the outlet temperature of the coolant, from 83.4°C to 81.2°C at solar noon. Heat flux transmitted through the absorber

portion between the tubes (fin) is made by conduction. It is in the form:

$$q_{u,cond} = \frac{2.k.\Delta T}{w}, \quad (-q_{u,cond} = -k.\vec{grad}T) \tag{17}$$

It is therefore obvious that this flow decreases when increasing w. It seems, according to this study, the value of w = 0.02m is most favorable to the design of our sensor. However, there are constraints of construction and market availability of this system type. We, therefore, opted for a distance w = 0.04m.

By setting the diameter of the tubes D=0.04m and the distance between pipes w=0.04m, it deduced that the solar collector is 15 tubes.

Figure 5.a: Variation of the useful flux and the outlet temperature as a function of the distance between the collector tubes at solar noon.

Thickness of the absorber E

For the optimal values of the parameters that we have studied, namely $\beta = 60°$, D = 0.04 m and w = 0.04 m, we will examine the effect of the thickness of the absorber plate on the two fundamental unknowns that are the useful heat flux and temperature at the outlet of the collector. Keeping these optimal values constant and by increasing Thickness of the absorber E from 0.001m to 0.015m, the maximum useful flux transferred to the coolant varies from 264.56 W/m^2 to 832.29 W/m^2, Fig.5.b. The increase of the thickness of the absorber E contributes to the increase
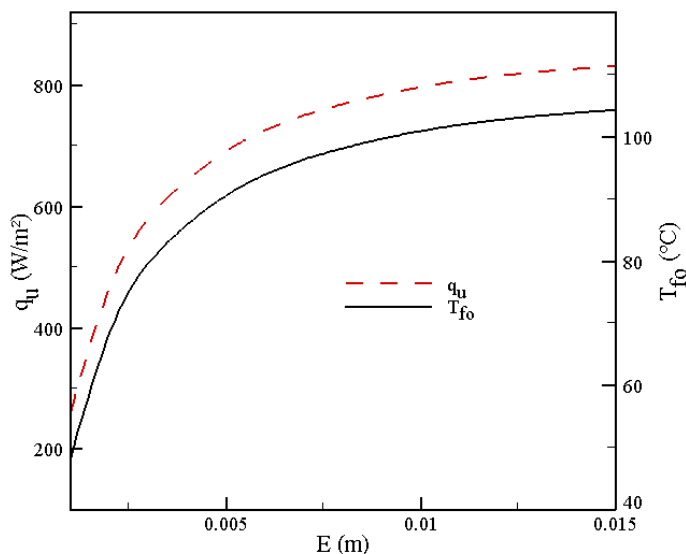
Figure 5.b: Variation of the useful flux and the outlet temperature as a function of the thickness of the absorber at solar noon.

of the outlet temperature of the heating fluid, from 48.1°C to 104.33°C at solar noon. The maximum value of the thickness E of the absorber available in the market, does not exceed E = 0.01m, value that we considered in our work.

• **The width L of the air layer**

The variation of the distance L between the glass and the absorber, slightly influence the thermal behavior of the solar collector. By varying L from 0.03 m to 0.08 m, the maximum useful heat flux transferred to the fluid increases from 797.73 W/m² to 819.87 W/m², Fig.6.a. The increase of the distance between the glass and the absorber L contributes to the increase in the temperature of the coolant, from 100.9 °C to 103.1 °C at solar noon. Note that, for this range of L, there is no important increase of heat flux or the outlet temperature. We must remember that the air layer is considered as an insulator until its thickness L does not exceed a limit value L ≤0.04m, value for which natural convection begins to develop. So, there will increase heat losses and it alters the sensor performance.

The optimal distance between the glass and the absorber is equal to 0.04 m.
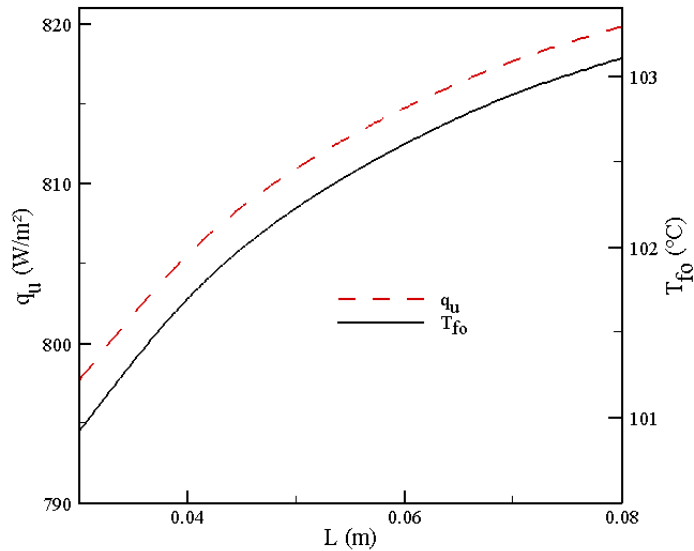
Figure 6.a: Variation of the useful flux and the outlet temperature as a function of the distance between the glass and the absorber at solar noon.
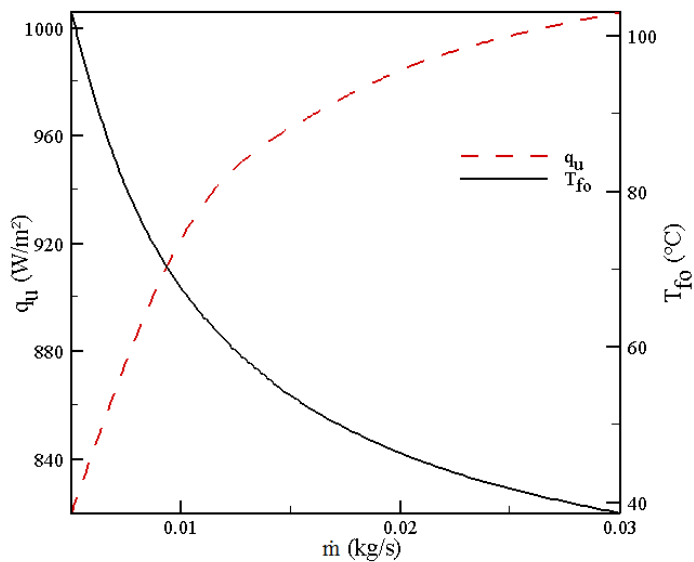

Figure 6.b: Variation of the useful flux and the outlet temperature as a function of the water flow rate at solar noon.

Water flow rate $\dot{m}$

The variation of the water flow rate $\dot{m}$, has a clearly effect on the thermal behavior of the solar collector, Fig.6.b. The increase of $\dot{m}$ from 0.005 kg/s to 0.03 kg/s creates a remarkable increase in the maximum useful heat flux transferred to the coolant that bounces from 819.87 W/m^2 to 1005.79 W/m^2. The increase of the water flow rate, also, creates a significant decrease of the output temperature of the heating fluid, from 103.1˚C to 38.5˚C at solar noon.

If we based our work on the heat flux to choose the optimal value of the flow rate $\dot{m}$, we have to take $\dot{m}$= 0.03 kg/s. On the contrary, if the choice was based on the outlet temperature, then the optimal flow rate is around 0.005 kg/s. Therefore we opted for a compromise where the choice of water flow rate $\dot{m}$= 0.009 kg/s to an optimum value of the outlet temperature of the heating fluid.

A second optimization work has been conducted by disrupting the values previously obtained for the parameters of the solar collector by $\pm 10\%$. The results of simulations show that these disturbances have not brought significant variations. The selected optimal configuration is given by Tab.5:

Table 5: Optimum geometrical configuration of solar collector.

β	D (m)	w (m)	E (m)	L (m)	$\dot{m}$ (kg/s)
60˚	0.04	0.04	0.01	0.04	0.009

Fig.7.a and fig.7.b show the evolution of the useful flux collected by the fluid and the temperature at the exit of the fluid over a period of 3 days. From midnight to 7:00 am, the useful heat flux decreases from 3.6 W/m^2 to 2.9 W/m^2 and the output temperature from 7.4˚C to 4.2˚C due to the heat losses towards the sky. An increase begins with the sunrise and causes the increase of the outlet temperature between 7:00 am and 1:00 pm, solar noon. The useful flux reaches its maximum value 908.4 W/m^2 between 11:00 am and 2:00 pm; it undergoes a rapid decline to reach the value of 1.5 W/m^2 at 5:00 pm featuring the sunset and therefore the absence of solar radiations. Similarly, the outlet temperature reaches its maximum value of 71.9˚C between 11:00 am and 2:00 pm then decreases till 14.3˚C at 5:00 pm. The outlet temperature of the heating fluid depends essentially on the useful flux.

3.2   *The PCM Optimization*

In the same manner as the last paragraph, we will conduct the study of the PCM optimization: the liquid fraction and the inlet temperature of the building variations
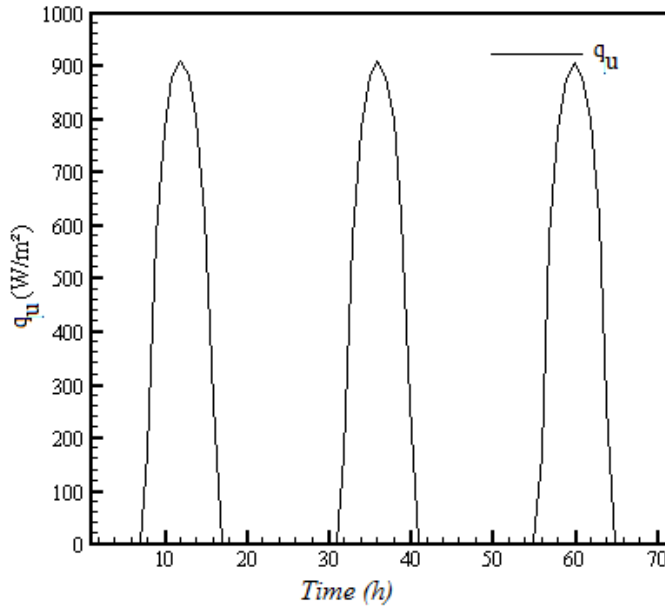
Figure 7.a: Typical useful flux of the solar collector during the month of January.

will be studied as functions of the thermo physical properties of the PCM.

Effect of the PCM thermal conductivity k_m

The variation of thermal conductivity k_m of the PCM has an appreciable effect on the thermal behavior of the system. By increasing k_m from 0.7 W/m K to 1.9 W/m K, the internal temperature of the building T_{in} reaches a maximum of 42°C around 4:00 pm, due to the thermal inertia of the PCM. This increase of temperature boosts the heat losses in the building. During the night, the internal temperature T_{in} decreases to 16°C for $k_m = 1.9$ W/m K less than the melting temperature $T_f = 22$°C, Fig.8.a. The increase of thermal conductivity k speeds up the destocking rate of the PCM, and led to the decrease of the liquid fraction f from 0.42 ($k_m = 0.7$ W/m K) to 0 ($k_m = 1.9$ W/m K) during the night, Fig.8.b. For a good thermal insulation to keep the internal temperature of the building close to the conditions of comfort, we take $k_m = 0.7$ W/m K.

Effect of the PCM specific heat capacity $c_{p,m}$

The specific heat $c_{p,m}$ represents the ability to store energy by the weight of the material; it allows the increase of the stocking rate of the PCM. This increase causes the decrease of the internal temperature of the building. Indeed, by increasing the
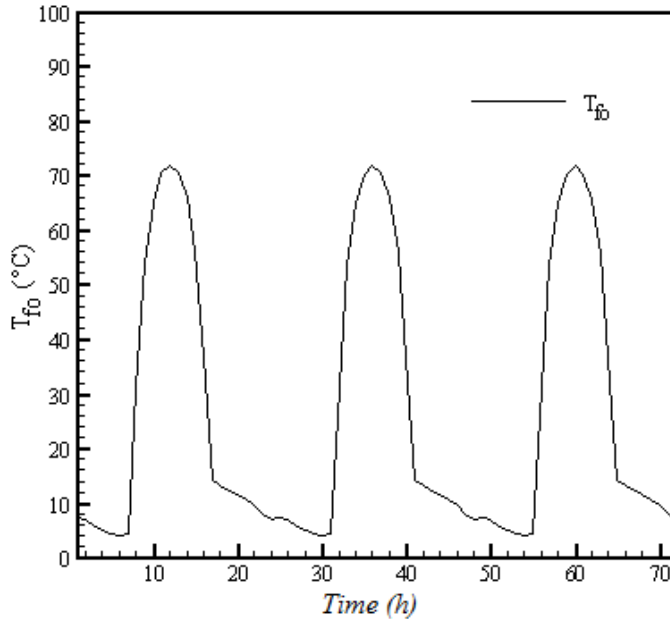
Figure 7.b: Typical outlet temperature of the solar collector during the month of January.

specific heat $c_{p,m}$ from 500 J/kg K to 1500 J/kg K, the internal temperature T_{in} decreases from 43˚C to 25˚C during the day and remains constant at T_f = 22˚C during the night, which gives a better thermal insulation of the building, Fig.9.a. The increase of the specific heat contributes to improving the storage/retrieval rate of the PCM, where the increase of the liquid fraction is from 0 ($c_{p,m}$ = 500 J/kg K) to 0.6 ($c_{p,m}$ = 1500 J/kg K) during the night, Fig.9.b. The highest specific heat $c_{p,m}$ = 1500 J/kg K gives the best performances of the PCM.

Effect of the PCM density ρ_m

By varying the PCM density from ρ_m = 1000 kg/m^3 to 2200 kg/m^3, the internal temperature T_{in} bounces between 1:00 pm and 10:00 pm for a maximum from 23˚C for ρ_m = 1000 kg/m^3 to 33˚C for ρ_m = 2200 kg/m^3 at 4:00 pm and remained stable at 22˚C during the night, Fig.10.a. The increase in density ρ_m also contributes to good storage of the PCM, where the decay of the liquid fraction f is from 0.6 to 0.14 during the night, Fig.10.b. For a good thermal insulation (in order to keep the internal temperature of the building under the conditions of comfort), we fixed ρ_m = 1800 kg/m^3.
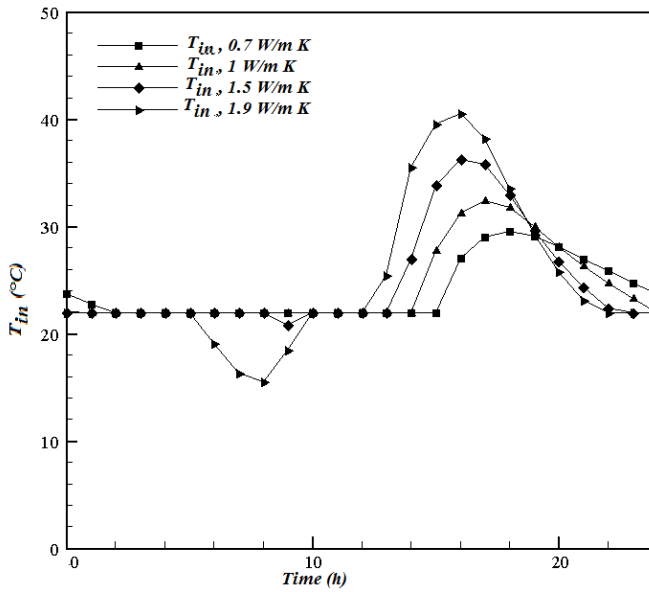
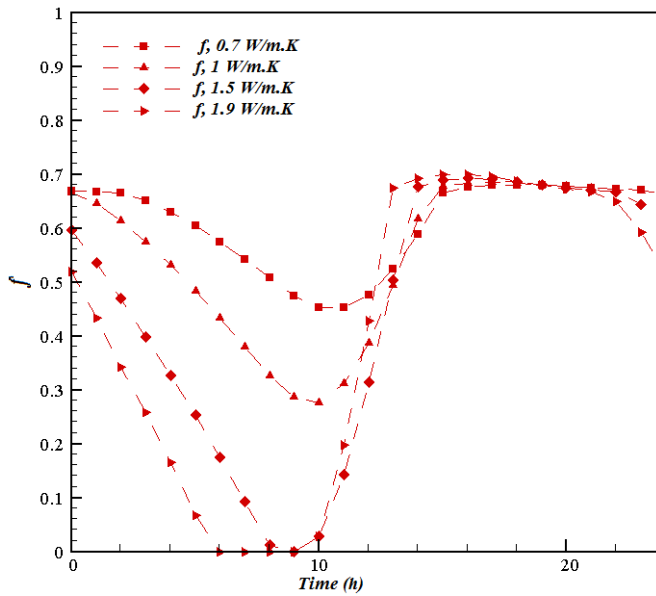Figure 8.a: Variation of the internal temperature as function of k_m.

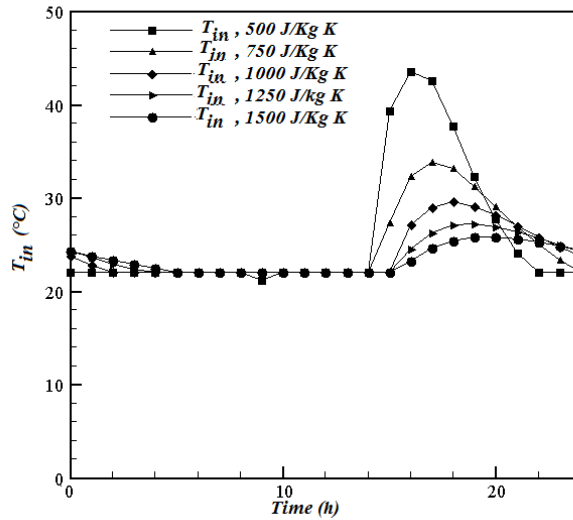Figure 8.b: Variation of the liquid fraction as function of k_m.

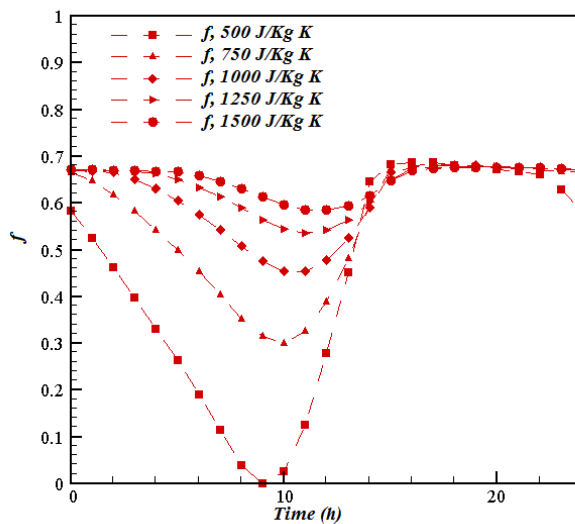Figure 9.a: Variation of the internal temperature as function of $c_{p,m}$.

Figure 9.b: Variation of the liquid fraction as function of $c_{p,m}$.

Fig.11 shows that :

- The internal temperature of the building increased from 22°C to 25°C while the ambient temperature increases from 2°C to 20°C, Fig.2, and the outlet temperature of solar collector increases from 4°C to 71°C, Fig.7.a.
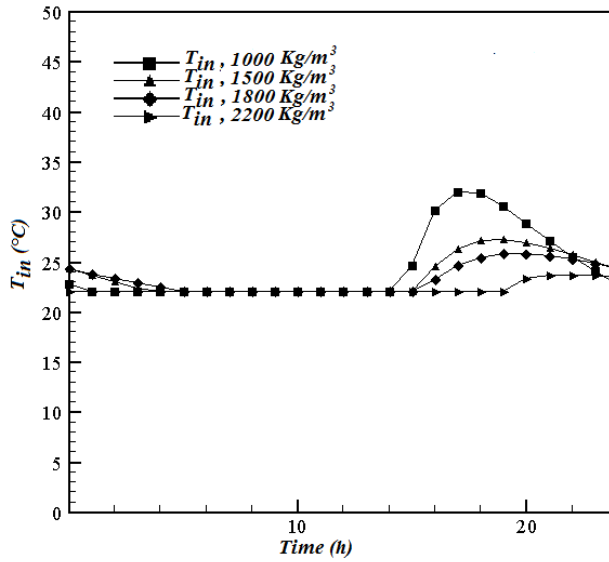
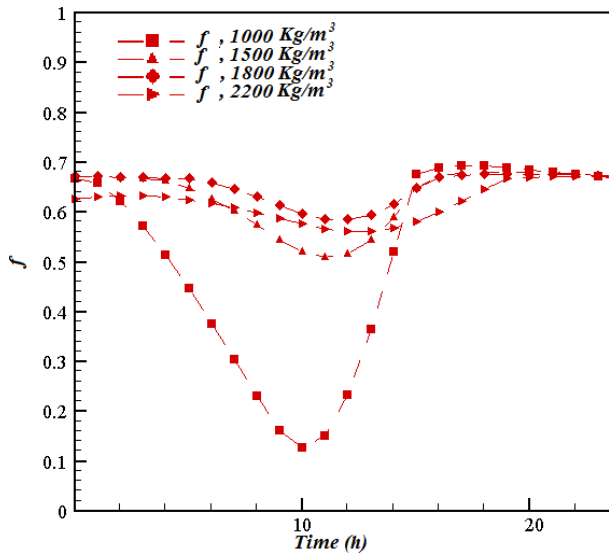Figure 10.a: Variation of the internal temperature as function of ρ_m.

Figure 10.b: Variation of the liquid fraction as function of ρ_m.

- The PCM layer receives a useful flux q_u of the solar collector, Fig.7.b which increases its temperature at 22˚C (melting temperature) and a first layer of

Table 6: Optimal configuration of the PCM.

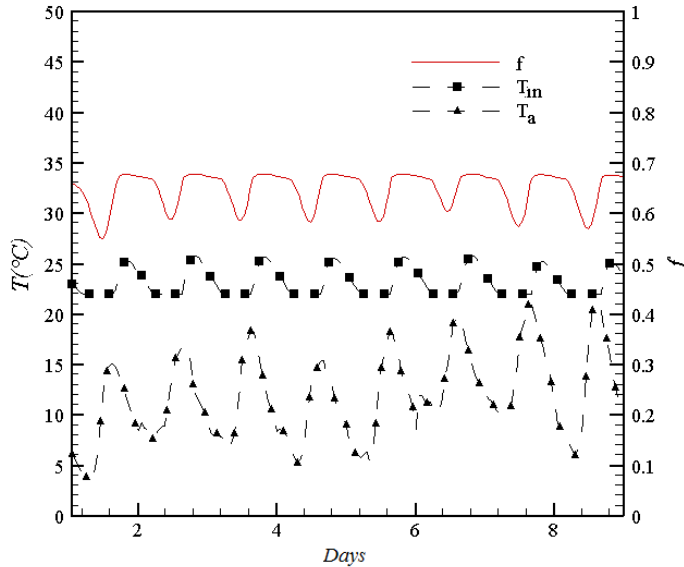| k_m (W/m K)	c_{pm} (J/kg. K)	ρ_m (kg/m³)	ΔH (KJ/kg)	T_f(˚C)
0.7	1500	1800	<u>200</u>	<u>22</u>

Figure 11: Internal building temperature T_{in} and liquid fraction f in a typical decade of January for the solar collector / PCM / concrete slab

the liquid phase appears, f=0.16.

• The presence of the PCM layer within the solar collector improves the heat storage in the material, and therefore, an increase in the liquid fraction.

• During the night, the outlet temperature of the solar collector is lower than that of the inner wall of the building. This temperature difference is due to the losses towards the sky.

• The decrease of the ambient temperature, after having reached a maximum, and the absence of solar radiations during the night, causes the decrease of the outlet temperature in solar collector, but the PCM provides its stored heat and ensures the heating. The internal temperature of the building remained stable at 22˚C.

- Cycle day/night allows the increase/decrease in the temperature of the building which varies between 22°C and 25.8°C during the month of January. The PCM solidifies and melts periodically and the liquid fraction f varies between 0.56 and 0.68.

- The fluctuation reduction in the internal temperature of the building is explained by the presence of the two phases of the PCM liquid and solid. The liquid fraction is always positive ($0.5 \leq f \leq 0.7$). The melting front does not reach the inner layer of concrete and does not reach the absorber of the solar collector. Therefore, there is presence of the two phases of the PCM, T_f =22°C heat source.

- The latent heat stored in the PCM layer maintains the temperature of the inside of the building close to the temperature of comfort (days and nights).

4   Conclusion

Dynamic simulations have shown that the optimization of the characteristic parameters of the solar collector allows an increase of its efficiency of 17%. The outlet temperature of the fluid increases from 56.7°C to 71.9°C. As, the useful flux increases by 351.76 W/m^2 at 908.4 W/m^2. The results show also that the outlet temperature of the heating fluid depends essentially on the useful heat flux. In addition to that, the optimization of thermo-physical parameters of the PCM ensures the conditions for thermal comfort for the building (day and night). Where, the internal temperature of the building increases from 22°C to 25°C, the ambient temperature increases from 2°C to 20°C and the outlet temperature of solar collector increases from 4°C to 71°C. Another advantage is that the presence of the PCM layer within the solar collector improves the heat storage in the material, and therefore, an increase in the liquid fraction.

References

Chassériaux, J. M. (1984): *Conversion Thermique du Rayonnement Solaire*, Edition Dunod, pp. 272.

Fong, K. F.; Lee, C. K.; Chow, T. T. (2012): Comparative study of solar cooling systems with building-integrated solar collectors for use in sub-tropical regions like Hong Kong. *Applied Energy*, vol. 90, pp. 189–195.

Hakem, S. A.; Kasbadji–Merzouk, N.; Merzouk, M. (2008): Performances journalières d'un chauffe-eau solaire. *Revue des Energies Renouvelables CICME'08*, pp. 153 – 162.

Handoyo, E. A.; Ichsani, D. (2013): The optimal tilt angle of a solar collector. *Energy Procedia*, vol. 32, pp. 166 – 175.

Gao, Y.; Zhang, Q.; Fan, R.; Lin, X.; Yu, Y. (2013): Effects of thermal mass and flow rate on forced-circulation solar hot-water system: Comparison of water-in-glass and U-pipe evacuated-tube solar collectors. *Solar Energy*, vol. 98, pp. 290–301.

Kosny, J.; Yarbrough, D.; Miller, W.; Petrie T.; Childs P.; Syed, A.; Leuthold, D. (2007): Thermal Performance of PCM-Enhanced Building Envelope Systems. *ASHRAE*.

Liu, B. Y. H.; Jordan, R. C. (1960): The interrelationship and characteristic distribution of direct, diffuse and total solar radiation. *Solar Energy*, vol. 4, no. 3, pp. 1-19.

Probst, M. C. M; Roecker, C. (2007): Towards an improved architectural quality of building integrated solar thermal systems (BIST). *Solar Energy*, vol. 81, pp. 1104–1116.

Patankar, S. V. (1980): *Numerical Heat Transfer and Fluid Flow*, Washington D.C. Hemisphere.

Prud'homme, R.; El Ganaoui, M. (2007): Solid/Liquid Phase Change: Recent Studies and Models. *Fluid Dynamics &Materials Processing,* vol.3, no. 2, pp. 161-172.

Rady, M.; Arquis, E. (2010): A Comparative Study of Phase Changing Characteristics of Granular Phase Change Materials Using DSC and T-History Methods. *Fluid Dynamics &Materials Processing,* vol. 6, no. 2, pp. 137-152.

Rahni, N. (1990): Estimation des Performances à Long Terme d'un Chauffe-eau solaire à thermosiphon par la méthode de la F Charte. *Mémoire de Fin d'Etude d'Ingéniorat*.

Soares, N.; Costa, J. J.; Gaspar, A. R.; Santos P. (2013): Review of passive PCM latent heat thermal energy storage systems towards buildings energy efficiency. *Energy and Buildings,* vol. 59, pp. 82–103.

Tadili, R.; Bargach, M. N. (2005): Une méthode d'estimation du rayonnement solaire global reçu par une surface inclinée. *La météorologie*, vol. 50, pp. 46–50.

Tagliafico, L. A.; Scarpa, F.; DeRosa, M. (2014): Dynamic thermal models and CFD analysis for flat-plate thermal solar collectors – A review, *Renewable and Sustainable Energy Reviews*, vol. 30, pp. 526–537.

Voller, V. R.; Cross, M.; Markatos, N. C. (1987): An Enthalpy Method for Convection/Diffusion Phase Change. *International Journal of Numerical Methods in Engineering*, vol. 24, no. 1, pp. 271 - 284.

Wei, L.; Yuan, D.; Tang, D.; Wu, B. (2013): A study on a flat-plate type of solar heat collector with an integrated heat pipe. *Solar Energy*, vol. 97, pp. 19–25.

Yang, Y.; Wang, Q.; Xiu, D.; Zhao, Z.; Sun, Q. (2013): A building integrated solar collector: All-ceramic solar collector. *Energy and Buildings,* vol. 62, pp. 15–17.